Controlling the symmetry of supercrystals formed by plasmonic core-shell nanorods with tunable cross-section

Cyrille Hamon,[a*] Claire Goldmann,[a] Doru Constantin[a*]

[a]Laboratoire de Physique des Solides, CNRS, Univ. Paris-Sud, Université Paris-Saclay, 91405 Orsay Cedex, France.

E-mail : cyrille.hamon@u-psud.fr, doru.constantin@u-psud.fr

Keywords: gold nanorods, supercrystals, self-assembly, small-angle X ray scattering, phase transformation.

Preparation of AuNR-Ag and experimental details

AuNR-Ag were prepared in aqueous solution by adjusting the the amount of silver precursor and ascorbic acid as reducing agent in the reaction mixture.[1] After mixing, samples were heated up to 60°C during 3h. An observation was made on the dimensional features of the AuNR@Ag nanoparticles depending on the silver feedstock. The gold nanorods may reshape during the synthesis which is likely related to the low thermal stability of gold nanorods.[2] We noted a 15 nm blue shift of the longitudinal plasmon band of the reference gold nanorods sample (i.e. without silver precursors) after heating the sample 3h at 60°C (**Figure S1A**) in agreement with a slight decrease in aspect ratio. In SAXS, a continuous shift of the form factor to smaller q values traduce an evolution of the AuNR dimensions (**Figure S1B**).
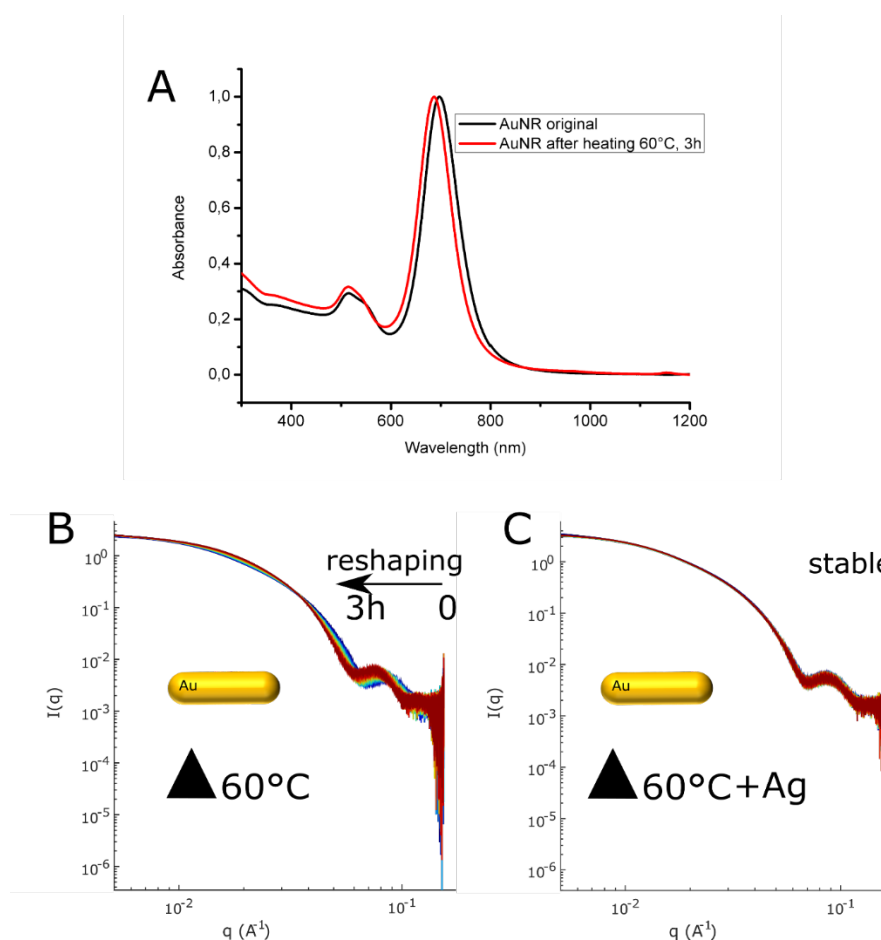

Figure S1: Morphological changes of gold nanorods during heating at 60°C. A) UV-Vis spectra of AuNR colloid before (black) and after (red) heating the suspension at 60°C during

3h. A blue shift of the longitudinal peak from 699 nm to 684 nm was determined. **B-C)** SAXS spectra representing the evolution of the form factor of dilute suspensions of AuNR during heating at 60°C. A) in absence or B) in presence of silver (0.2 eq Ag/Au ratio). The temporal resolution was 10 min.

This phenomenon was however not observed when silver was introduced in the reaction mixture, suggesting a complete coverage even at a low silver to gold molar ratio of 0.2 (**Figure S1C**). Therein, the stability of the SAXS spectra over time corresponds to the growth of a subnanometer layer of Ag which had a negligible influence on the initial form factor of the nanoparticles. The preservation of the gold nanorod core can be understood from a kinetic point of view in which the fast deposition of the silver shell hinders any thermal reshaping.

Simulation of the optical properties of the nanocrystals:

Simulated extinction spectra were calculated by the boundary element method (BEM), using the MNPBEM toolbox developed in the MATLAB environment.[3] The particle is described as a gold spherocylindrical core with 14,7 nm in diameter and 44.5 nm in length, encased in a silver square-based prismatic shell with side lengths W for the base and with height L. Two parameters were adjusted in the simulations to fit the experimental spectra, namely the dimension of the prismatic shell (W and L) and the degree of rounding on the corner. The best fits were obtained with a rounding of 0.4 for sample 1 to 5 and a rounding of 0.15 for the thickest samples (**6** and **7**) which is related to the evolution of the particles from a spherocylinder to a cuboid with sharper edges as more silver is deposited. The dimensions of the prismatic shell for all samples were in agreement with results obtained by TEM and SAXS (see **Table 1** in the manuscript).
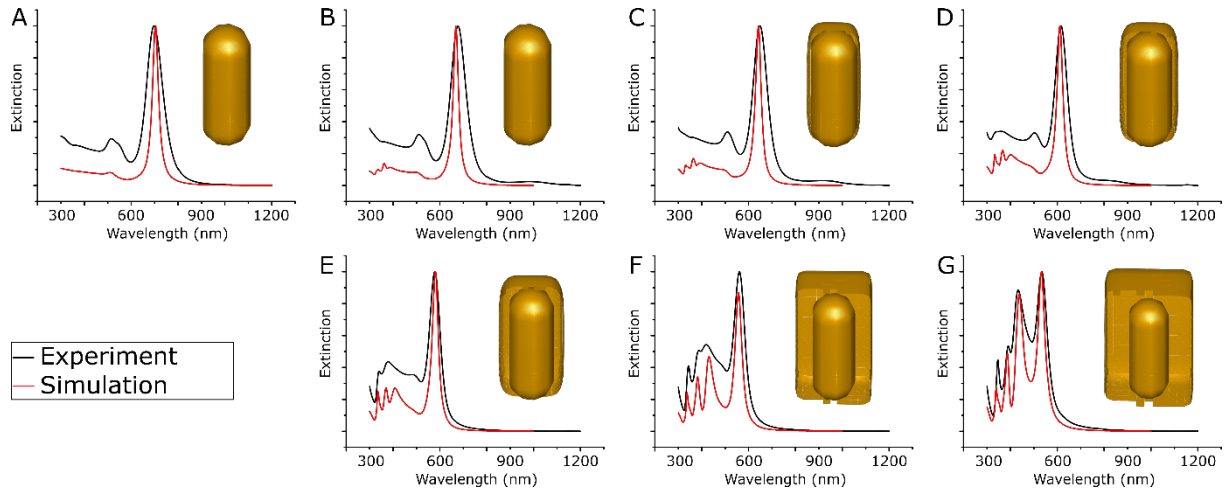
Figure S2: Modelling the optical properties of the nanoparticles by BEM. From A) to G) UV/Vis spectra representing the original data (black) compared with the model (red) for sample 1 to 7 respectively. In each case, the nanoparticles are represented with a half shell, so the gold nanorod core is visible. These shapes were used in the calculation by the BEM approach after defining the dielectric properties.

Details on SAXS experiments

The composite objects (AuNR-Ag) are best described as gold spherocylinders with radius R and straight length H contained within straight rectangular prisms made of silver, with side lengths A, B and C, see **Figure S3a**.

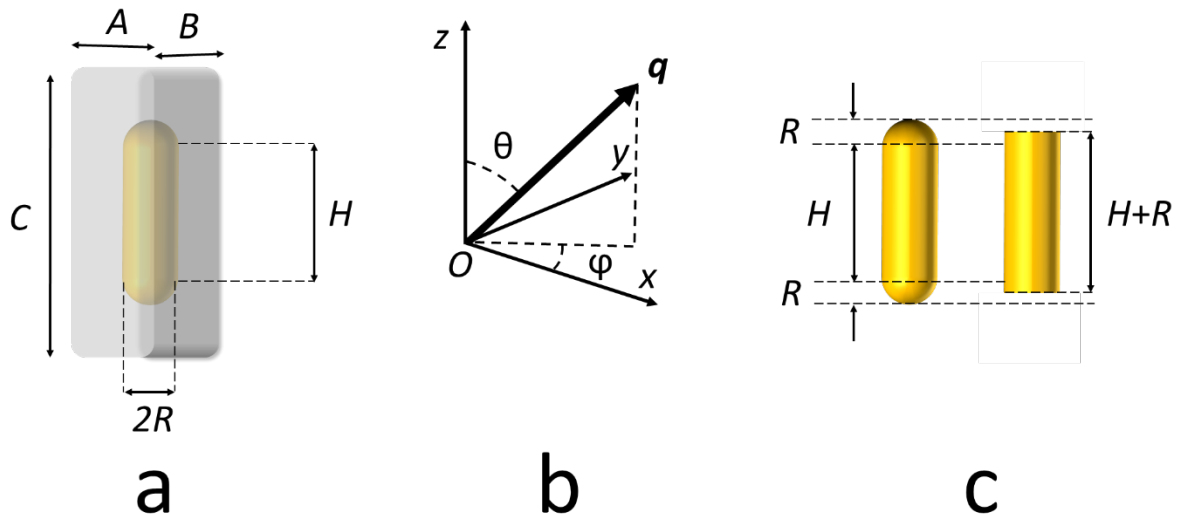**Figure S3**: a) Diagram of the objects. b) Scattering geometry. c) The equivalent cylinder (with length $H'=H+R$) of a spherocylinder.

Informed by the TEM images, we assume that $A = B < C$ and that the spherocylinders are centered within the prisms (they share z as symmetry axis). The scattering signal I of a dilute colloidal solution of such objects as a function of the scattering vector q can be written as:

$$I(q) = \frac{scale}{V_{tot}} \langle |G|^2 \rangle_{\theta,\varphi} + bkg,$$

where *scale* is a scale factor proportional to the volume fraction of the objects in solution, V_{tot} is the total volume of the particle, *bkg* is a residual background term, G is the (anisotropic) form factor of the particle (defined below) averaged over the polar and azimuthal angles θ and ϕ, respectively.

$G = c_1 f_1 + c_2 f_2 + c_3 f_3 = \Delta\rho_{sm} \, ABC \, f_1(A, B, C, q, \theta, \varphi) + \Delta\rho_{cs} \, 2\pi R^2 L \, f_2(R, H, q, \theta) +$

$\Delta\rho_{cs} \, 4\pi R^3 \, f_3(R, H, q, \theta).$

On the right-hand side of the equation, we expanded the c_i constants in terms of the particle sizes defined above and the scattering length density (SLD) density contrast between shell (silver) and the surrounding medium (water) $\Delta\rho_{sm} = \rho_s - \rho_m$ and between core (gold) and shell, $\Delta\rho_{cs} = \rho_c - \rho_s$. The individual form factors f_i depend on the particle dimensions (A, B, C, H and R) and on the scattering geometry (absolute value q and orientation angles θ and ϕ of the scattering vector q with respect to the particle reference system, see **Figure S3b)**.

Only the form factor of the prism f_1 depends on the azimuthal angle ϕ; the contributions of the cylindrical stem f_2 and of the end caps f_3 exhibit full azimuthal symmetry and thus only depend on the polar angle θ. Thus, the full orientational average can be decomposed as:

$\langle |G|^2 \rangle_{\theta,\varphi} = \frac{1}{2} \int_0^\pi d\theta \sin\theta \, \langle |G|^2 \rangle_\varphi$, where $\langle |G|^2 \rangle_\varphi = c_1^2 \langle f_1^2 \rangle_\phi + [c_2 f_2 + c_3 f_3]^2 +$

$2c_1 [c_2 f_2 + c_3 f_3] \langle f_1^2 \rangle_\phi,$

and:

$$f_1(A, B, C, q, \theta, \varphi) = \text{sinc}\left(\frac{1}{2}qA \sin\theta \cos\phi\right) \text{sinc}\left(\frac{1}{2}qB \sin\theta \sin\phi\right) \text{sinc}\left(\frac{1}{2}qC \cos\theta\right)$$

$$f_2(R, H, q, \theta) = 2 \, \text{sinc}\left(\frac{1}{2}qH \cos\theta\right) \frac{J_1(qR \sin\theta)}{qR \sin\theta}$$

$$f_3(R, H, q, \theta) = \int_0^1 dt \cos\left[q\left(\frac{L}{2} + Rt\right)\cos\theta\right] (1 - t^2) \frac{J_1[qR \sin\theta\sqrt{1-t^2}]}{qR \sin\theta\sqrt{1-t^2}},$$

where the analytical expression above for the end-cap contribution f_3 can be found, for instance, in[4]. Numerical evaluation of this term is however very time-consuming, due to the integral over t. We found empirically that the form factor of a spherocylinder with parameters H and R is well reproduced by a simple cylinder with parameters $H'=H+R$ and R, see **Figure S3c**. We have used this simplification throughout the analysis.

The geometrical parameters H and R are obtained by fitting the intensity scattered by gold nanorod solutions, without silver addition and corroborated with the TEM results. They are kept fixed for all particles based on that particular nanorod batch. The width $W=A=B$ and length $L=C$ of the prisms are optimized for each sample (**1** to **7**).

We account for the polydispersity by introducing a homothetical size distribution: all dimensions are scaled by a parameter λ with respect to their reference values $A_0=B_0$, C_0, H_0, R_0 (in which case the scattered signal is $I_0(q)$, corresponding to $\lambda=1$) and λ is distributed along a Gaussian:

$$d(\lambda) = \frac{1}{\sqrt{2\pi}\,p} \exp\left[-\frac{1}{2}\left(\frac{\lambda-1}{p}\right)^2\right].$$

Scaling all sizes by λ or the scattering vector q by the same factor preserves the signal, up to a λ^6 prefactor (easily understood if we recall that the scattered intensity is proportional to the particle volume squared.) The polydisperse signal can then be obtained as:

$$I_{\text{avg}}(q) = \int d\lambda \, \lambda^6 d(\lambda) \, I_0(\lambda q)$$

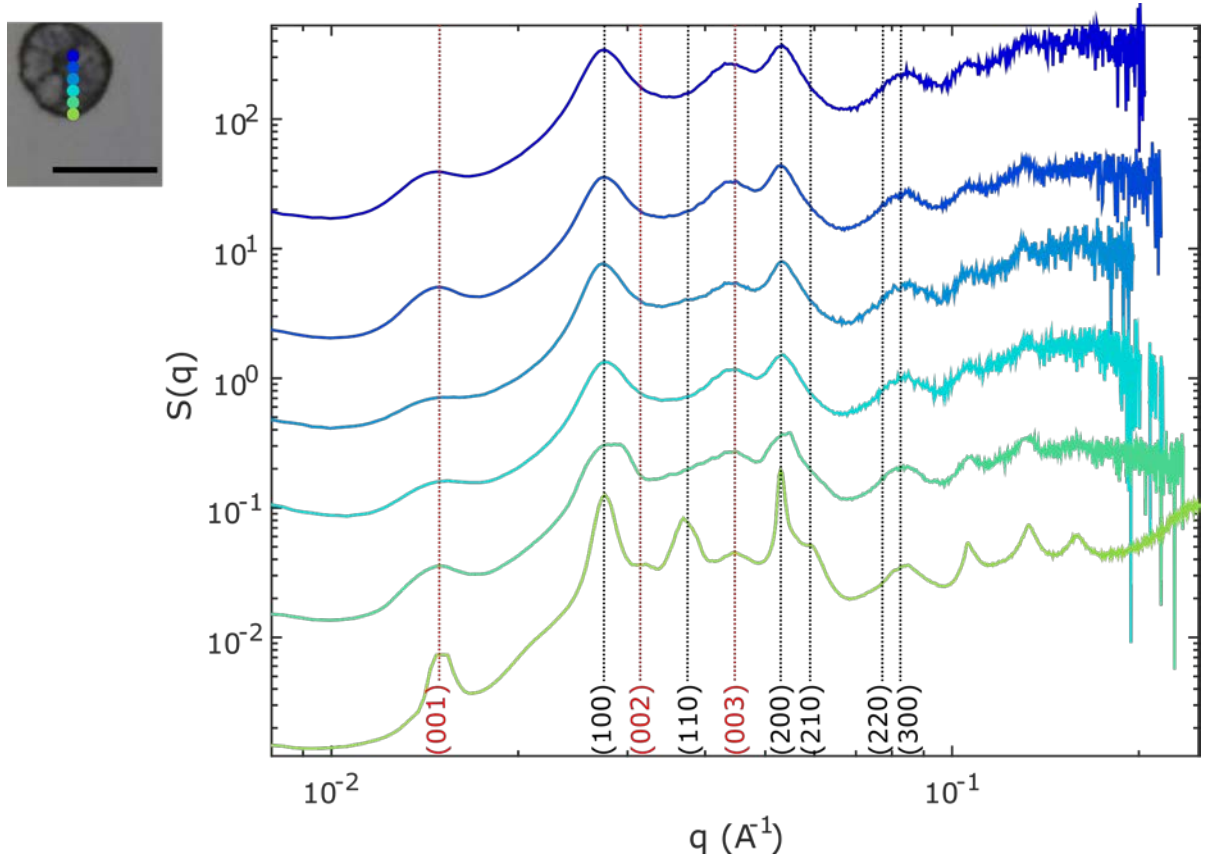The fit parameters given in the main text correspond to: $W=A_0=B_0$, $L=C_0$, PDI=p.

Figure S4: Spatially resolved SAXS on CTAB-4 supercrystals thin films. Insets shows a photograph of the deposit with scale bar being 0.5 cm. Insets shows photographs of the deposit with the scale bar being 0.5 cm in all images. Beam positions corresponding to the SAXS measurement are marked on the image, with the same color code as for the SAXS curves. Dotted vertical lines indicate the expected positions of the Bragg peaks.

Figure S5. Photograph of the sample holder before SAXS measurement. The beam irradiated the sample perpendicularly to the substrate. The thin films composed of AuNR-Ag supercrystals were placed on a sample holder and scanned by moving the holder in respect to the SAXS beam in the direction of the arrow.
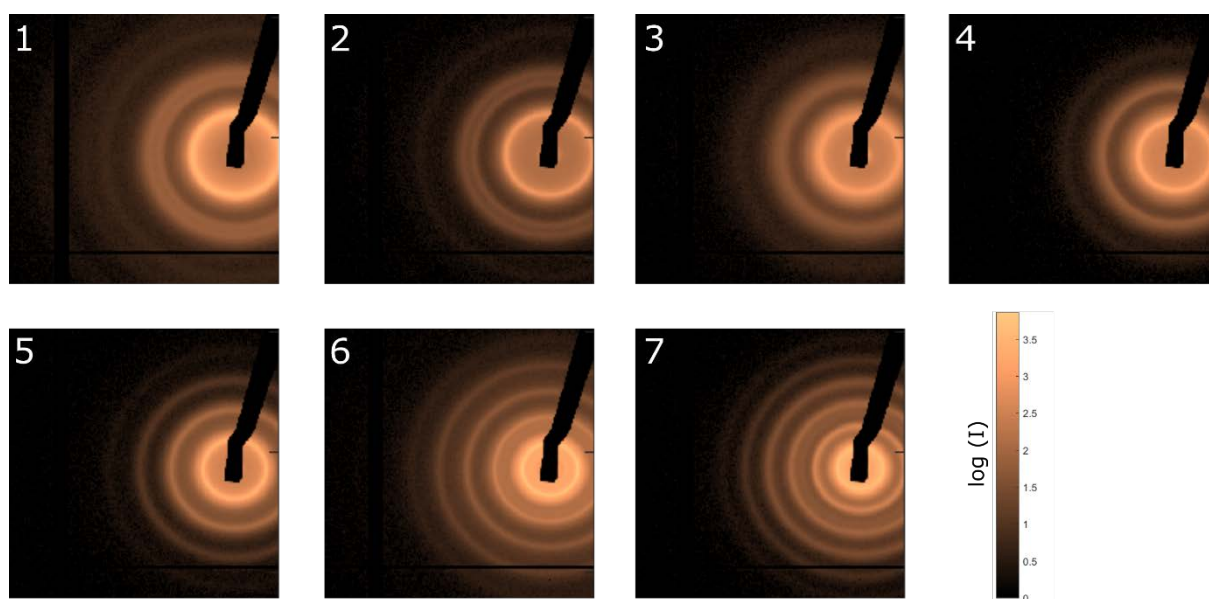

Figure S6: Representative 2D SAXS patterns of AuNR-Ag monolayers obtained from samples **1** to **7.**
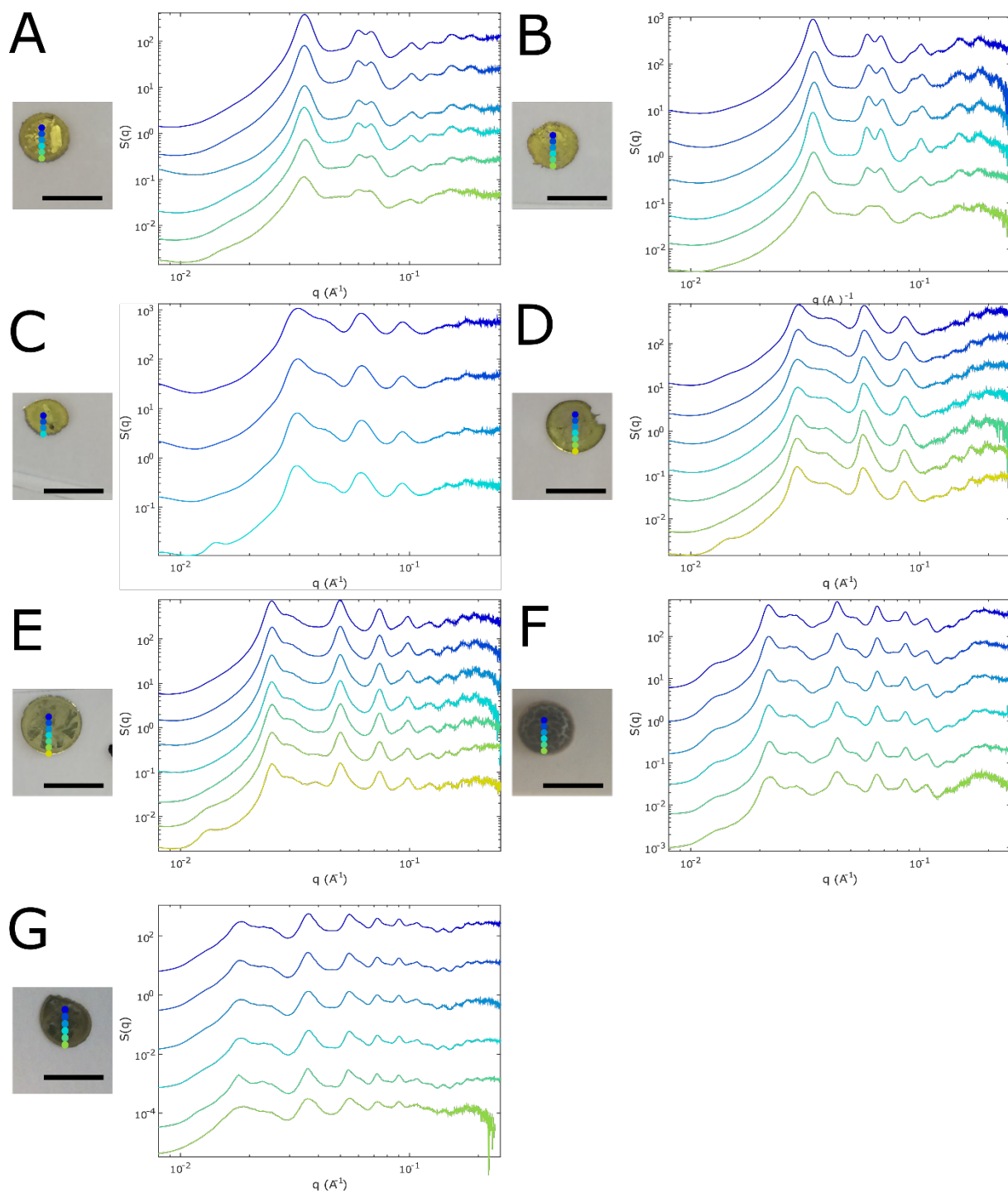
Figure S7: Spatially resolved SAXS on AuNR-Ag supercrystals thin films. All AuNR-Ag were functionalized with MUDOL before deposition. A) AuNR, B) AuNR-0.9Ag, C) AuNR-1.9Ag, D) AuNR-3.0Ag, E) AuNR-8.1Ag, F) AuNR-11.7Ag, G) AuNR-17.8. Insets shows photographs of the deposit with scale bar being 0.5 cm in all images. Positions where SAXS measurement have been made are indicated on the image.
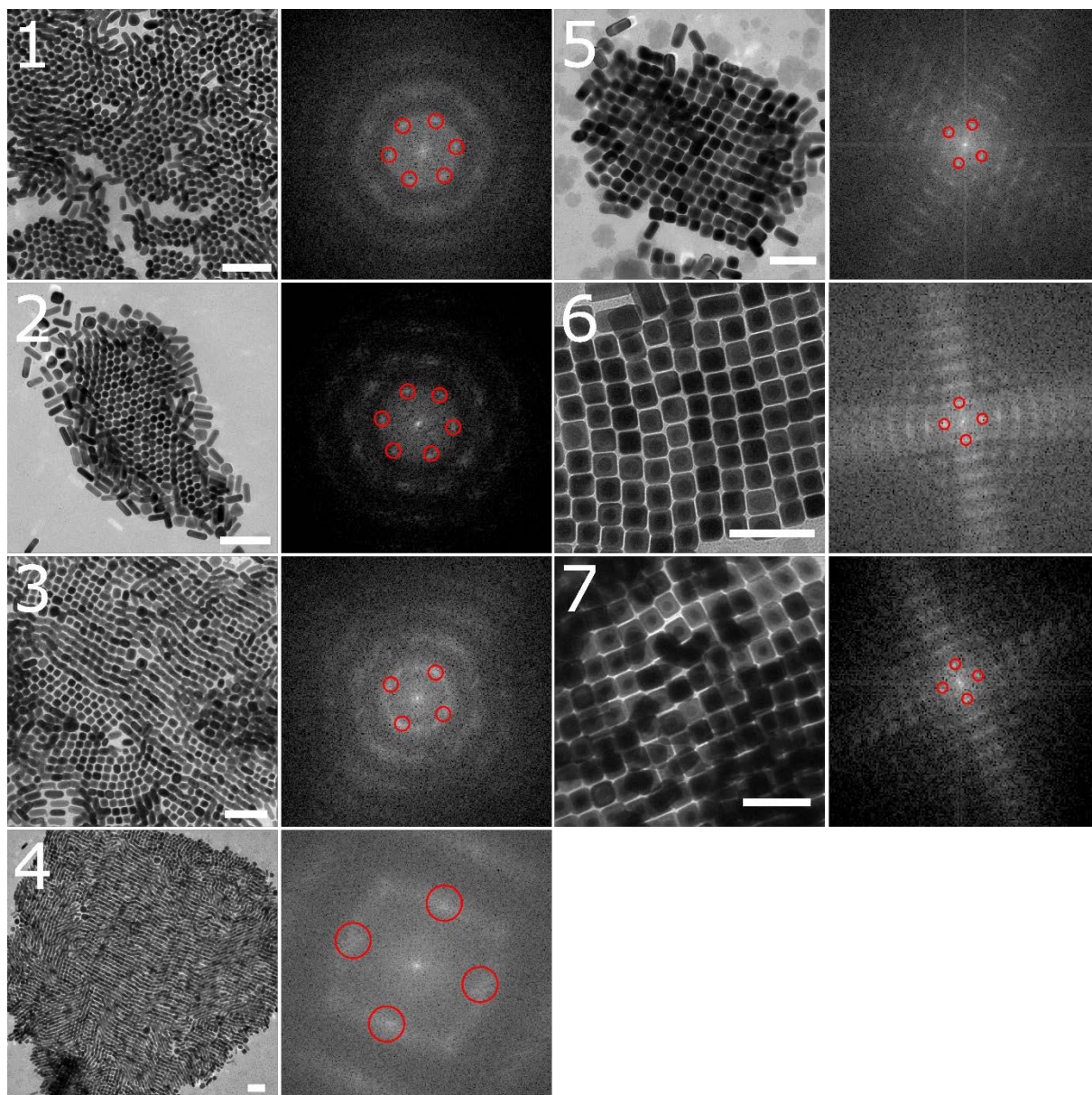
Figure S8: Determination of the critical silver thickness at which the in-plane symmetry switches from hexagonal to square. TEM images and associated FFT of AuNR-Ag monolayers obtained from samples **1** to **7**. Scale bar on TEM images is 100 nm.
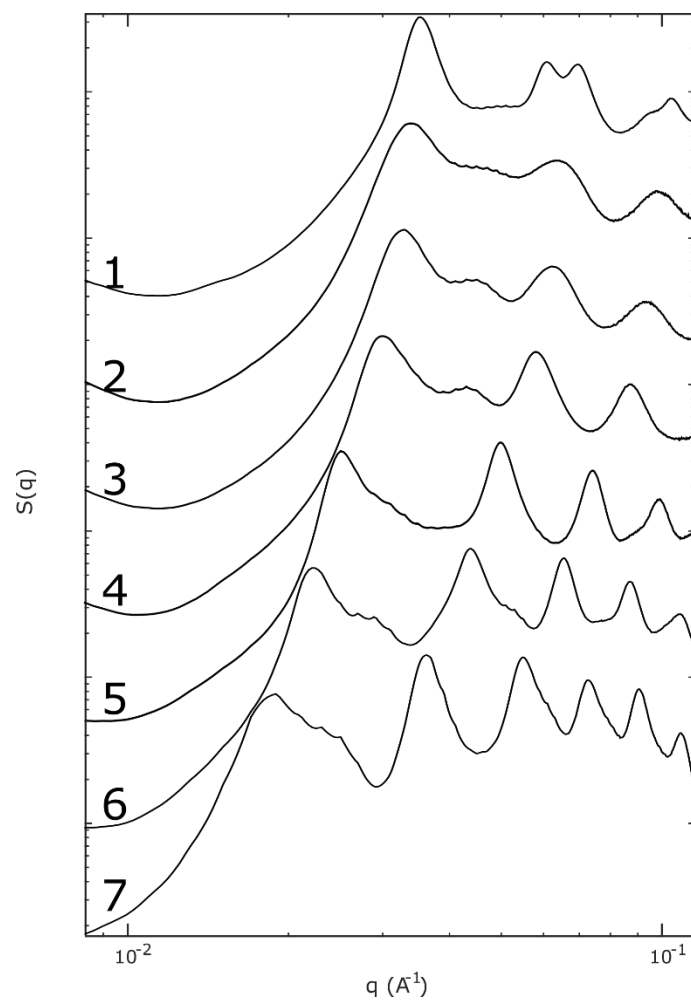
Figure S9: Complementary SAXS spectra obtained from AuNR-Ag supercrystals dried in capillaries. The numbers juxtaposed to the spectra correspond to the sample labels defined in the manuscript.
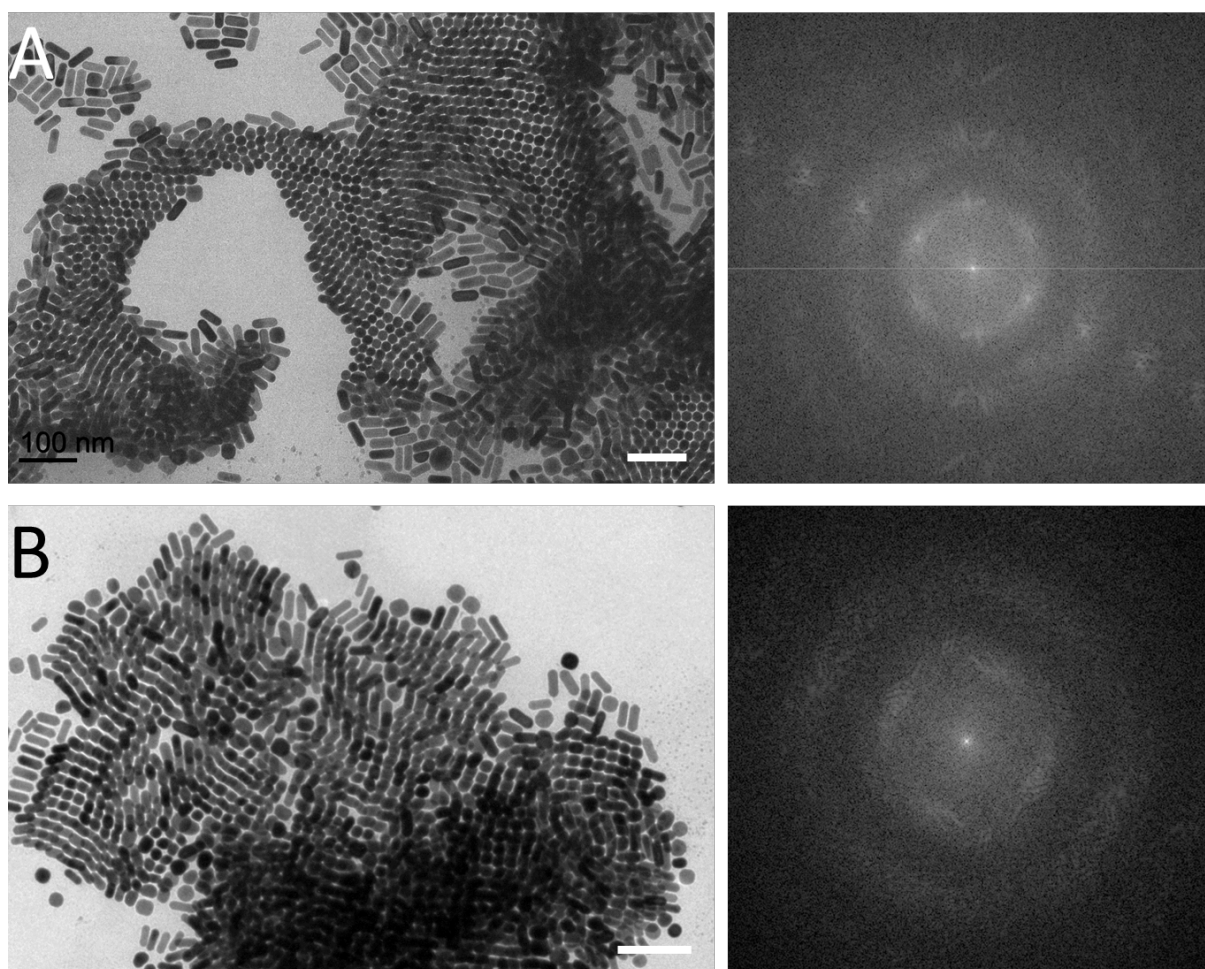
Figure S10: TEM images of AuNR (L = 45.4 nm, W = 14.8 nm) and AuNR-Ag monolayers and corresponding FFT. **A**) Hexagonal ordering in AuNR assemblies. **B**) In plane square arrangement of AuNR-Ag prepared with a silver to gold ratio of 0.4. Scale bar on all images is 100 nm.

Figure S11: TEM images of AuNR (L = 39.5 nm, W = 10.4 nm) and AuNR-Ag monolayers and corresponding FFT. **A**) Hexagonal ordering in AuNR assemblies. **B**) In plane square arrangement of AuNR-Ag prepared with a silver to gold ratio of 0.4. Scale bar on all images is 100 nm.
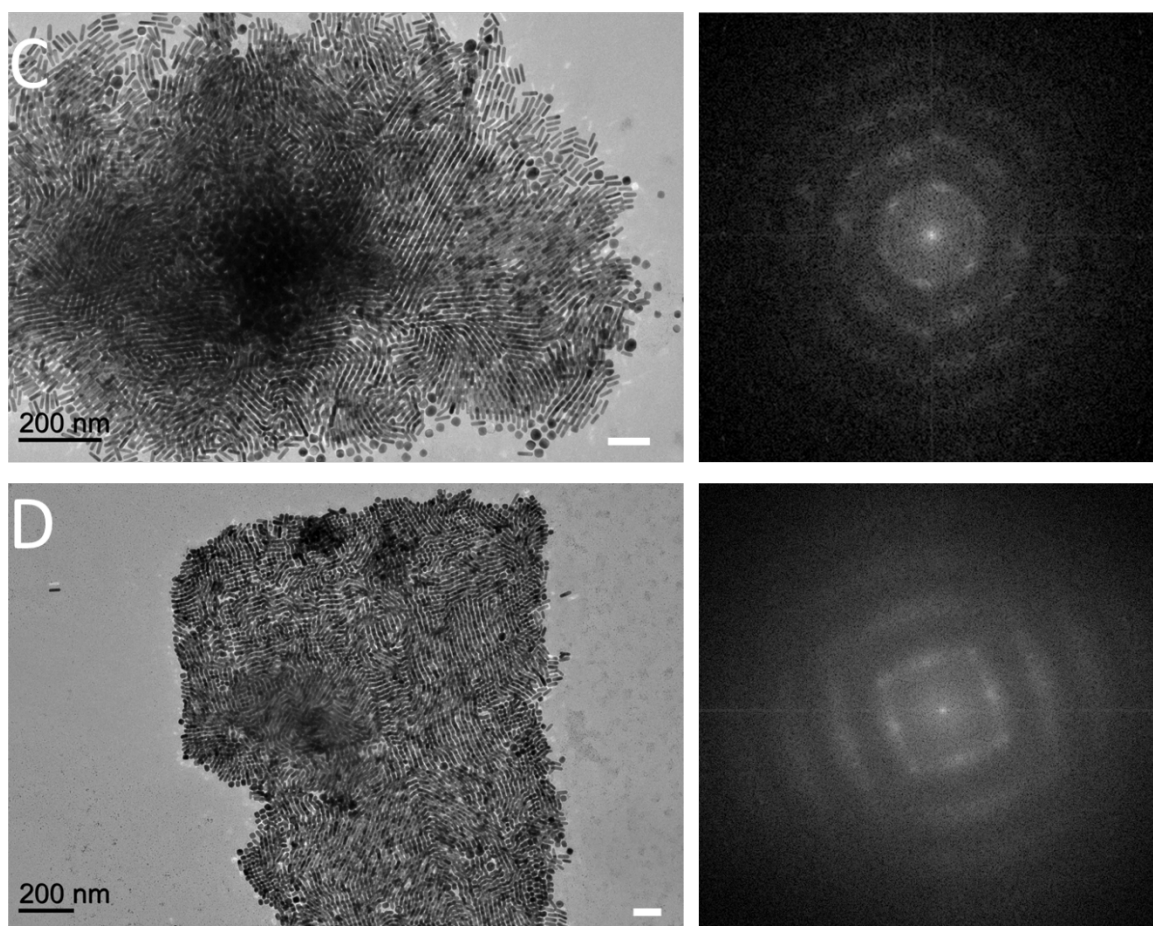
Estimation of the amount of silver needed to turn a gold nanorod with regular octagonal cross-section into a square-shaped one.
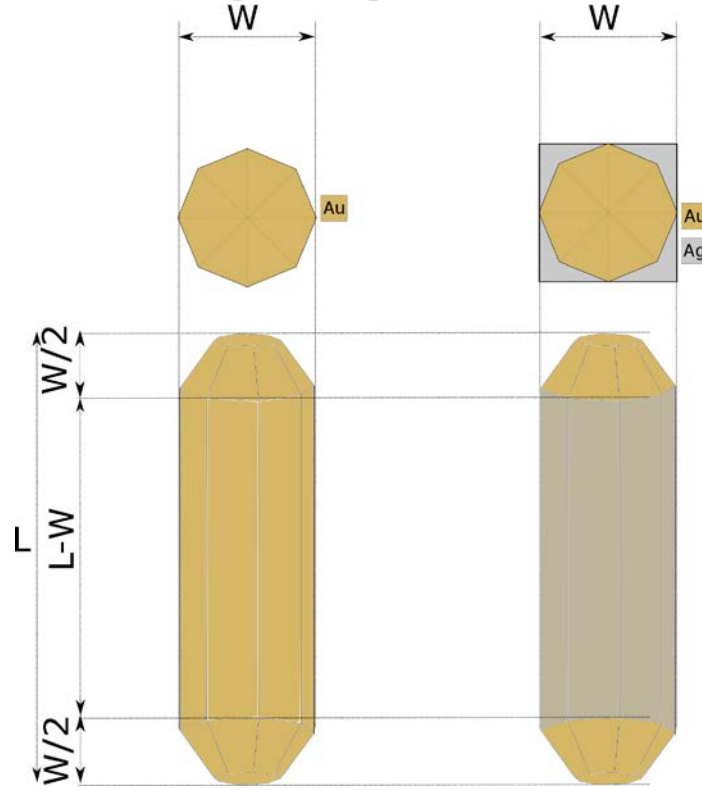

Figure S12: Illustration describing a gold nanorod encased in a square prismatic silver shell. The volume of silver per particles can be estimated by subtracting the volume of the cuboidal shell by the volume the core.

The in-plane orientation of the gold nanorod within the silver shell **(Figure S12)** is determined from high-resolution TEM images from the literature.[5] V_t define the threshold volume at which a gold nanorod with regular octagonal cross-section turn into a square-shaped one, in the configuration illustrated **Figure S12** and can be written as:

$$V_{\text{gold-covered by silver}} = \frac{\sqrt{2}}{2} \times W^2 \times (L - W)$$

$$V_{\text{cuboid}} = (L - W) \times W^2$$

$$V_t = V_{\text{cuboid}} - V_{\text{gold-covered by silver}}$$

This volume can be converted into moles ($n_{t(1\text{particle})}$) considering the bulk density of silver (D_{silver}) and its molar mass (M_{silver}) as:

$$n_{t(1particle)} = \frac{V_t \times D_{silver}}{M_{silver}}$$

We plotted $n_{t(1particle)}$ against rods of varying length and width in **Figure S13**.
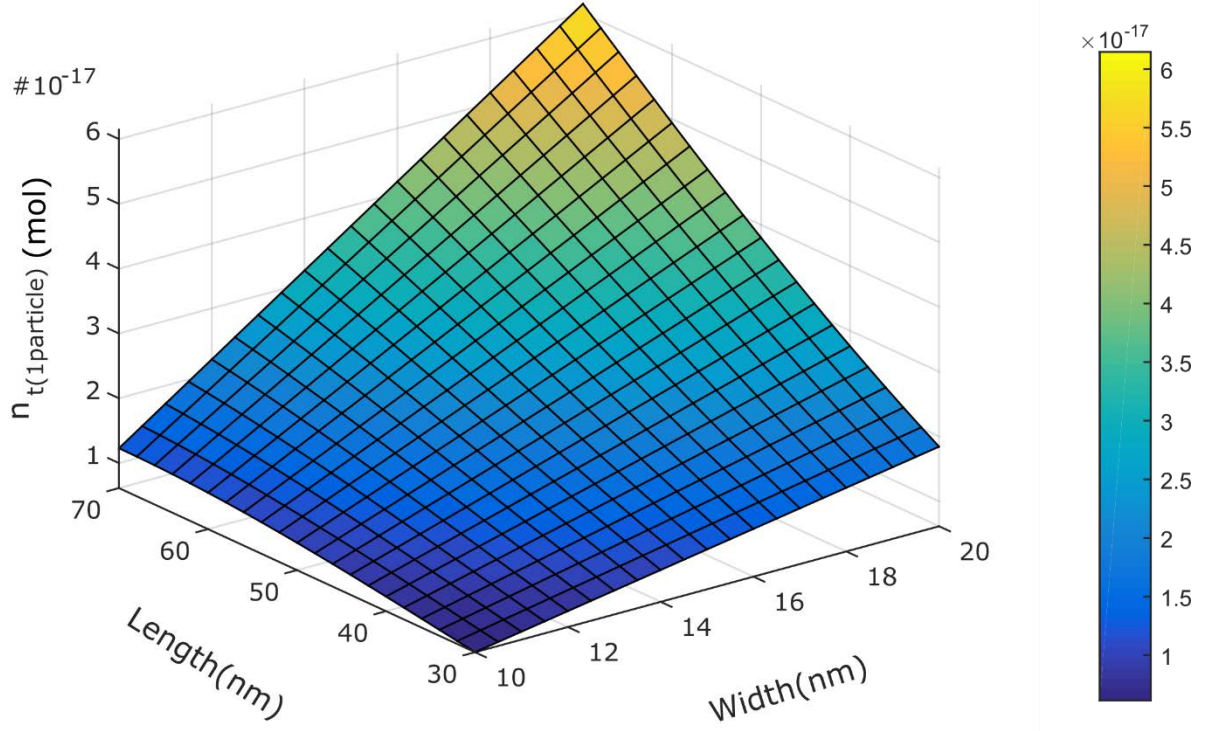

Figure S13: Three-dimensional surface plot representing the minimum amount of silver needed to turn a gold nanorod with regular octagonal cross-section into a square-shaped one ($n_{t(1particle)}$), plotted against varying rods length and width.

The number of particle in a synthesis (ParticlesNumber) can be determined by considering the ratio of the total amount of gold in the solution (nAu^0), obtained from the absorbance at 400 nm,[6] and the quantity of gold in one gold nanorod (n_{AuNR}) which is calculated similarly as $n_{t(1particle)}$, albeit considering the bulk density of gold (D_{gold}) and its molar mass (M_{gold}). Note that we approximated the volume of a gold nanorod as a hemispherically capped cylindrical nanorods with an octagonal cross section. These can be traduced as the following expression:

$$n_{AuNR(1particle)} = \frac{\left(\frac{\sqrt{2}}{2} \times W^2 \times (L - W) + \frac{\pi}{6} \times W^3\right) \times D_{gold}}{M_{gold}}$$

$$ParticlesNumber = \frac{nAu^0}{n_{AuNR(1particle)}}$$

$n_{t(1\ particle)}$ can be then scaled up, by multiplying this quantity to the particle number in solution defining n_t corresponding to the threshold quantity of silver which turns the cross section of all particles in solution into squares.

$$n_t = n_{t(1particle)} \times ParticlesNumber$$

n_t can be compared to the known quantity ($n_{silver(exp)}$) of silver added experimentally during the synthesis of the AuNR-Ag. In the case of the gold nanorods considered in the manuscript (L=44.5 nm, W=14.7 nm), we plotted the ratio of $n_{silver(exp)}$ by n_t against the molar silver to gold ratio determined experimentally in **Figure S14**. This graph shows that from a silver to gold ratio of 0.4, we should observe AuNR-Ag rods with squared cross-section which is confirmed experimentally.
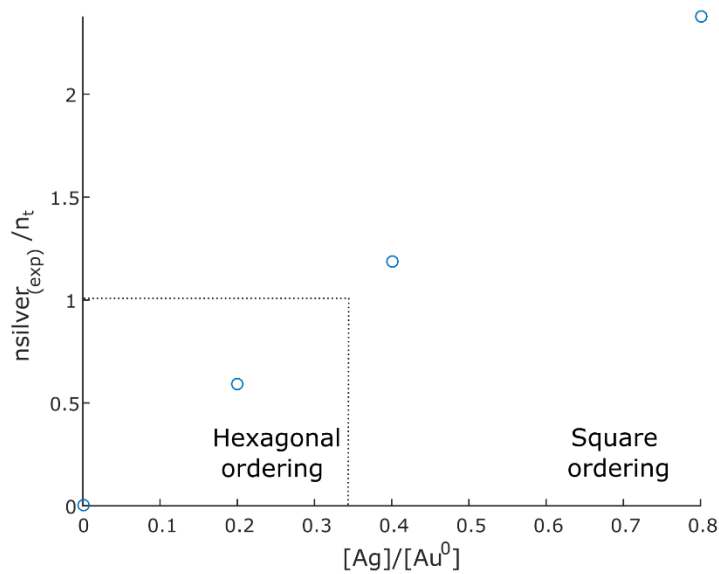
Figure S14: Graph representing the ratio of $n_{silver(exp)}$ by n_t plotted against the molar silver to gold ratio determined experimentally.

References

[1]   a) Y. Okuno, K. Nishioka, A. Kiya, N. Nakashima, A. Ishibashi, Y. Niidome, *Nanoscale* **2010**, 2, 1489; b) M. Tebbe, C. Kuttner, M. Mayer, M. Maennel, N. Pazos-Perez, T. A. F. König, A. Fery, *J. Phys. Chem. C* **2015**, 119, 9513; c) K. Park, L. F. Drummy, R. A. Vaia, *J. Mater. Chem.* **2011**, 21, 15608.

[2]   H. Petrova, J. Perez Juste, I. Pastoriza-Santos, G. V. Hartland, L. M. Liz-Marzan, P. Mulvaney, *Phys. Chem. Chem. Phys.* **2006**, 8, 814.

[3]   U. Hohenester, A. Trügler, *Comput. Phys. Commun.* **2012**, 183, 370.

[4]   H. Kaya, *J. Appl. Crystallogr.* **2004**, 37, 223.

[5]   S. Gómez-Graña, B. Goris, T. Altantzis, C. Fernández-López, E. Carbó-Argibay, A. Guerrero-Martínez, N. Almora-Barrios, N. López, I. Pastoriza-Santos, J. Pérez-Juste, S. Bals, G. Van Tendeloo, L. M. Liz-Marzán, *J. Phys. Chem. Lett.* **2013**, 4, 2209.

[6]   L. Scarabelli, A. Sánchez-Iglesias, J. Pérez-Juste, L. M. Liz-Marzán, *J. Phys. Chem. Lett.* **2015**, 6, 4270.